Electrochemistry

Received: September 15, 2015
Accepted: January 14, 2016
Published: April 5, 2016

The Electrochemical Society of Japan

http://dx.doi.org/10.5796/electrochemistry.84.219

Comprehensive Paper

Electrochemistry, **84(4)**, 219–223 (2016)

Ultrathin Porous NiO Nanoflake Arrays on Nickel Foam as Binder-free Electrodes for Supercapacitors

Qing LIU,[a] Qinglong YAN,[a] Shuang WU,[a] Jieqiang WANG,[a,*] and Huakun LIU[b]

[a] *School of Materials Science and Engineering, University of Jinan, Jinan 250022, P. R. China*
[b] *Institute for Superconducting and Electronic Materials, University of Wollongong, NSW 2522, Australia*

* *Corresponding author: msewangjq@ujn.edu.cn*

ABSTRACT

NiO nanopowders and NiO/nickel foam (NF) hybrid were synthesized by microwave hydrothermal method and the following heating process. NiO nanopowders show the morphology of microspheres (diameter is about 3 μm), which are composed of porous nanoflakes. NiO/NF hybrid shows a porous nanoflakes array structure, the thickness of nanoflakes is 10 nm. Electrochemical measurements indicate that the maximum specific capacitance of NiO nanopowders is about 85.4 F/g at a scan rate of 5 mV/s, while this value is up to 234.8 F/g for NiO/NF hybrid. Electrochemical impedance spectrum (EIS) data show that the R_s and R_{ct} values of NiO/NF hybrid (1.9 Ω and 0.25 Ω) are smaller than that of the NiO nanopowders which are coated on nickel foam (3.6 Ω and 0.3 Ω). In conclusion, the ultrathin porous NiO/NF is directly used as a binderfree supercapacitor electrode, which exhibited significantly improved supercapacitor performance compared to NiO nanopowders.

Keywords : Nanopowders, Nanoflakes, Microwave Hydrothermal, Binderfree

1. Introduction

Over the past decade, supercapacitors (also known as electrochemical capacitors) have attracted much attentiondue to high power density, short charging time and long lifespan, etc. Supercapacitors are of interest in energy storage applications such as uninterruptible back-up power supplies, hybrid electronic vehicles, and renewable energy systems.[1] They're efficient energy storage devices with special performance that bridges the gap between conventional capacitors and batteries. Supercapacitors can be classified into three types based on their charge storage mechanism and electrode materials. The one is electric double layer capacitor (EDLC), whose electrode materials are almost carbon active materials, it's mainly because carbon active materials have more excellent performance such as larger specific surface area, lower price, easier to make and environmental friendlinees. The other is pseudocapacitor, pseudocapacitors store charges by redox reactions on the surface of the electrode, whose electrode materials are almost transition metal oxides and conductive polymer. Another is asymmetric supercapacitor, which is the combination of the both above and it is a kind of new energy storage device.[2–4] EDLCs use reversible adsorption of ions between the electrode and electrolyte interface to store charges, but its low energy density limits their applications.[5] Pseudocapacitors use highly reversible chemical adsorption stripping or redox reactions on the surface of the electrode to store charges.[6] Transition metal oxides (TMOs) as the electrode materials got extensively research, especially ruthenium oxide (RuO_2), due to its conductivity and specific capacitance in acidic electrolyte is significantly higher than the other electrode materials, besides, its stable properties can generate higher specific energy.[7] Nevertheless, the high cost and toxic nature of RuO_2 has limited its practical production and commercial applications. Hence, some other alternative electrode materials with low cost, abundant resources, nonpollution and excellent performance, such as NiO,[8,9] Co_3O_4[10,11] and MnO_2[12,13] have been received tremendous interests in recent studies.

NiO is one of the promising materials as electrode of supercapacitors owning to its high theoretical capacity (2573 F/g within 0.5 V), cost effectiveness and sufficiently large pseudo-capacitive behavior, in addition, its preparation method is simple.[14] NiO nanopowders have diverse morphologies, such as nanoneedles,[15,16] microspheres composed of nanoflakes, flower-like nanoparticles[17–19] and hollow microspheres[20–23] etc. These various morphologies result in distinct difference in their electrochemical performance, especially the microsphere composed of nanoflakes, which provides much shorter pathways for electron and ion transport, improves the diffusion of electrolyte, enhances kinetics and activity leading to excellent electrochemical performance.[24] So far, a lot of reports have indicated NiO with different nanostructured configurations and morphologies has their own features. For instance, Liu et al.[25] reported that supercapacitor regarded urchin-like NiO nanoparticles as electrode is pseudocapacitance nature, showing the maximum specific capacitance is 290 F/g, the specific capacitance only decays 25% after 500 continuous charge-discharge cycles. Vijayakumar et al.[26] noticed that NiO nanoflakes synthesized by microwave method at microwave radiation of 240 W for 5 min in a household microwave oven (ONIDA) and then calcinated at 300°C for 60 min exhibit maximum specific capacitance of 401 F/g at current density of 0.5 mA/cm^2. Ranga Rao et al.[27] reported that urchin-like porous NiO synthesized via the microwave hydrothermal method generates more pathways for ions to improve the transmission capacity maximum specific capacitance of 337 F/g at a scan rate of 2 mV/s. However, it is also noted that the active sites decreased due to the introduction of a conductive agent and a polymer binder during the electroactive powder particles coated on conductive substrates still seriously limit their performance. In order to solve this problem, a new concept is to grow electroactive nanostructures on conductive substrates directly to be used as integrated electrodes for supercapacitors.[28] Therefore it will be of great significance to develop effective and facile methods to grow electroactive materials directly on conductive substrates for high performance supercapacitors.

There are various methods to synthesize NiO nanopowders, such as traditional hydrothermal method,[29] microwave hydrothermal method, homogeneous precipitation[30] and sol-gel method.[31] Contrasting to traditional hydrothermal method, the microwave hydrothermal method[32,33] has many advantages, such as fast heating, efficient energy conservation, selective heating and environmental

protection. In addition, this method has smaller temperature gradient and no heating hysteresis phenomenon in the heating process. Therefore, microwave hydrothermal method as the new facile heating method has received tremendous interest recently.[34]

In this work, we have successfully prepared NiO nanopowders and growed ultrathin porous NiO nanoflake arrays on nickel foam into NiO/NF hybrid by microwave hydrothermal method. The electrochemical performances of NiO nanopowders and NiO/NF hybrid, in 6.0 M KOH electrolyte, have been reported and discussed. Moreover, a comparison was made between them to demonstrate that NiO/NF hybrid might hold higher potential as the electrode for high-performance energy storage devices.

2. Experimental Method

2.1 Materials synthesis

NiO/NF hybrids were synthesized by a microwave hydrothermal method and the following heating process. All the reagents were analytical grade and used without further purification. Deionized water was used during all the experimental processes. Before the synthesis, two pieces of nickel foams (2 cm × 2 cm) were washed with deionized water and ethanol for several times. The nickel sulfate ($NiSO_4{\cdot}6H_2O$) and urea were mixed in the ratio 1:2, configured to 60 mL aqueous solution and the concentration of Ni^{2+} ion is 0.1 M. After vigorous stirring for 30 min, as-obtained transparent reaction solution was transferred into a 100 mL double-walled vessel, which has an inner liner and a cover made of Teflon PFA and an outer high strength sleeve. After processing the nickel foams were immersed in the vessel. The vessel was sealed and maintained in a Microwave Accelerated Reaction System (MARS-5, CEM Corporation, USA) at 160°C for 30 min with the ramping rate of 15°C/min. While in the reaction solution without addition of nickel foam produced NiO nanopowders. In order to improve the dispersion, suitable amount of PEG-4000 was added as the surfactant in the process of NiO nanopowders preparation. After the reaction was completed, the nickel foams were taken out and cleaned by deionized water and ethanol to remove the loosely products attached on the surface. The resultant precipitates in the solution were centrifuged with deionized water and ethanol. After that, the nickel foams and precursor precipitates were dried at 70°C for 48 h. Then, the nickel foams loaded with the as-grown precursors and precursor powders were calcined at 400°C for 2 h at a heating rate of 5°C/min in nitrogen to get the NiO/NF hybrids and NiO nanopowders.

2.2 Material Characterization

Crystallite structure of the NiO was characterized by a D8-Advance X-ray powder diffractometer (Bruker, Germany) with Cu Kα radiation (λ = 0.154056 nm). The thermal behavior of the precursor was examined by employing thermogravimetric and differential scanning calorimetry (TG-DSC) on a STA409-EP comprehensive thermal analyzer (Netzsch, Germany) with a heating ramp of 10°C/min from room temperature to 700°C in nitrogen. Scanning electron microscopy (SEM) images were acquired on a QUANTA FEG250 scanning electron microscope (FEI, USA) to characterize the morphology of the samples.

2.3 Electrode preparation and electrochemical measurement

Preparation of the working electrode as follows: the NiO nanopowders, activated carbons and polytetrafluoroethylene (PTFE) were mixed in a mass ratio of 80:15:5 and dispersed in ethanol to produce the homogeneous slurry. Then the slurry was coated onto one half of the nickel foam substrate (1 cm × 2 cm), the mass loading of active materials is about 2 mg/cm^2. Relatively, the mass loading of NiO/NF is about 1.5 mg. After being dried in vacuum drying oven at 80°C for 8 h, the as-formed electrodes loaded with the active material were pressed to sheets. All the electrochemical performances were performed on an Autolab CHI604D electrochemical workstation. The electrochemical measurements were carried out using a three-electrode electrochemical cell in a 6.0 M KOH, the obtained NiO powder-based electrode or hybrid array-based electrode as the working electrode, platinum as the counter electrode, saturated calomel electrode as the reference electrode, respectively. The electrochemical properties of the working electrodes were evaluated by cyclic voltammetry (CV) and electrochemical impedance spectroscopy (EIS) in 6.0 M KOH solution. CV measurements were performed at different scan rates in a potential window of −0.2 V to 0.5 V. EIS measurements were recorded at open circuit potential with a frequency loop from 500 kHz to 0.01 Hz. The specific capacitance was calculated from the CV curves based on the following equation:[35]

$$C = \frac{S}{\Delta V \cdot \nu \cdot \mathrm{m}} \tag{1}$$

Where C (F/g) is specific capacitance, S (cm^2) is area of CV curve, ΔV (V) is working voltage, ν (mV/s) is scan rate, m (g) is the mass of active materials, respectively.

3. Results and Discussion

3.1 Phase transformation

The XRD patterns of precursor of NiO are shown in Fig. 1. It shows that XRD patterns of these precursors were all the same, proving the same product. The diffraction peaks at 11.35°, 33.46° and 59.98° correspond to the (003), (101) and (110) planes of α-$Ni(OH)_2$. The absence of any other peaks confirms the phase purity of the $Ni(OH)_2$. The α-$Ni(OH)_2$ is obtained by free precipitation from a solution reaction at 160°C. In this temperature, urea hydrolyzes gradually and releases NH_3 and CO_2. The resulting weak alkaline condition is believed to create numerous nucleation sites for the formation of α-$Ni(OH)_2$. The self-assembly process of α-$Ni(OH)_2$ was proved by monitoring the continuous morphological evolutions of α-$Ni(OH)_2$. With increasing reaction time, the green precipitate was producted gradually. The related reaction formulas can be written as follows:

$$CO(NH_2)_2 + H_2O \rightarrow 2NH_3 + CO_2 \tag{2}$$

$$Ni^{2+} + 2NH_3 + 2H_2O \rightarrow \alpha\text{-}Ni(OH)_2\downarrow + 2NH^{4+} \tag{3}$$

TG-DSC studies were carried out to assess the follow-up calcination process of the as prepared α-$Ni(OH)_2$. As depicted in Fig. 2, the precursor undergoes a weight loss of 32% in two-step weight loss process involving the dehydration and decomposition of precursor. The weight loss (5%) below 300°C is ascribed to the removal of adsorbed water and the evaporation of the intercalated water molecules.[36] The subsequent weight loss (27%) with a strong exothermic peak at 350–580°C arises from the loss of water and

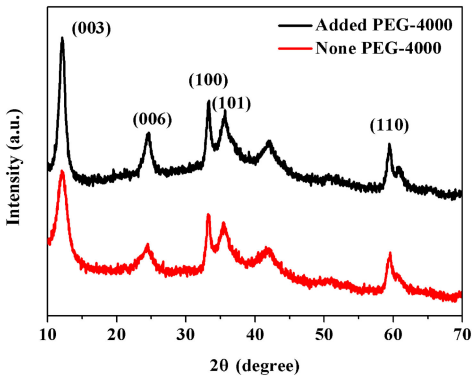

Figure 1. (Color online) XRD pattern of precursor with PEG-4000 added (black) and none (red).

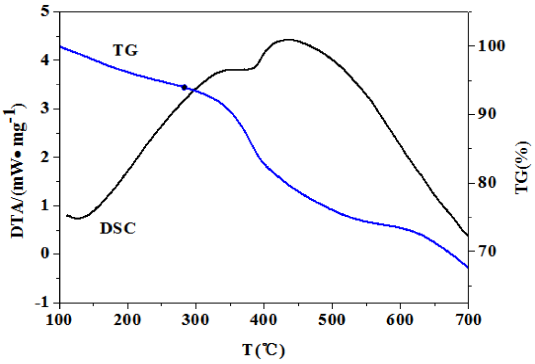

Figure 2. (Color online) TG (blue) and DSC (black) curves of the as-prepared precursors.

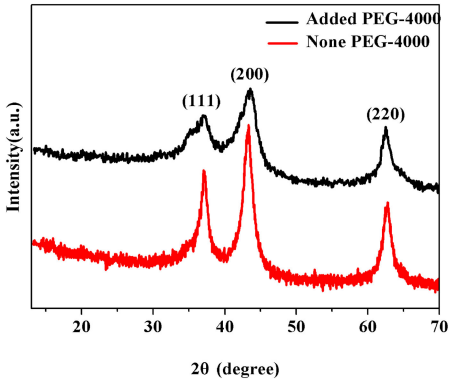

Figure 3. (Color online) XRD pattern of NiO nanopowders with PEG-4000 added (black) and none (red).

CO_2 generated by the dehydroxylation and decomposition of precursor.[37] The sharp weight loss around 380°C is an indication of complete conversion of α-Ni(OH)$_2$ to NiO. At higher temperature, no obvious weight loss indicates that there is no additional phase or structural change in NiO. Therefore, in order to obtain the NiO with high purity, 400°C is chosen as the calcination temperature. Figure 3 shows the XRD patterns of NiO black powders calcined at 400°C for 120 min. The diffraction peaks at 37.16°, 43.22° and 62.80° correspond to the (111), (200) and (220) indexed to the rocksalt-type NiO, and the lattice parameters are $a = 4.177$ Å. The absence of any other peaks confirms the complete decomposition of the precursor to the high purity of the NiO.

3.2 Morphological and structural studies

The morphological and structural features of the precursors, as-synthesized NiO nanopowders and NiO/NF hybrid are characterized by SEM. Figure 4a displays the image of the as-obtained precursor with crossing stack form of nanosheets. The homogeneous environment provided by microwave hydrothermal method makes the secondary aggregate relatively uniform in scales. Figure 4b displays the obtained NiO calcined at 400°C with 0.5 g PEG-4000, which composed of many microspheres (diameter is about 3 µm) consisted of porous nanoflakes self-assembly accumulation. The formation mechanism of the NiO porous nanoflakes is the release of isometric water steam and phase transition of α-Ni(OH)$_2$ in the process of calcination. Moreover, hydrogen bonding of PEG can wrap up NiO surface by affinity effect preventing the coagulation of nanometer particles, improving its dispersion and the stability of reaction solution, and helping the NiO nanoparticles self-assemble into porous nanoflake microspheres. In addition, within such unique porous nanoflakes, the open and free interspaces provide more active sites, thereby improving the utilization effect of electrode

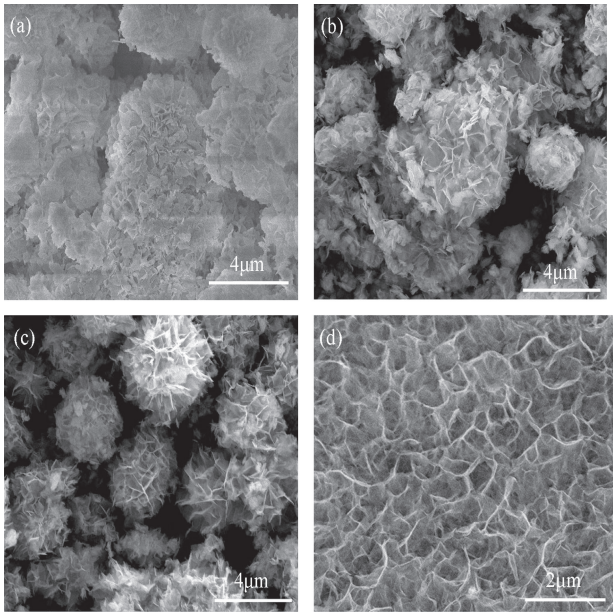

Figure 4. SEM images of the as-obtained precursor (a), the obtained NiO calcined at 400°C with 0.5 g PEG-4000 (b), the obtained NiO calcined at 400°C with none added PEG-4000 (c) and the NiO/nickel foam hybrid calcined at 400°C (d).

materials. In Fig. 4c, the NiO prepared without surfactant has irregular shape and its size is not uniform, the agglomeration is relatively serious. From Fig. 4d, it can be seen clearly that NiO attached on nickel foam has an array structure consisting of loose nanoflakes with regular clear boundary and larger porosity. This structure is beneficial to accelerate the transmission of ions and process of charge and discharge. The binder-free electrode architecture has the following important advantages for high-performance supercapacitors. First, the NiO nanoflakes directly contact with nickel foam can enhance the electrical conductivity of the electrode and shorten the diffusion paths of the electron. Second, the porous feature of NiO nanoflakes increases the amount of electroactive sites and facilitates transport of the electrolyte. Third, In the hybrid electrode, the Ni foam can act both as a buffering matrix to accommodate the local volumetric expansion/contraction of NiO nanoflakes upon longterm cycling, and as a conductive core to provide efficient transport of electrons for stable Faradaic redox reactions of the NiO. Thus, the morphological and electrochemical changes of NiO nanoflakes induced by charge/discharge cycling are greatly reduced, ensuring a remarkably enhanced cycling performance of the NiO/NF hybrid electrode.[38]

3.3 Electrochemical studies

To evaluate the potential of the NiO nanopowders and NiO/NF hybrids acting as electrodes for supercapacitors, the electrochemical capacitive behavior was first elucidated by the CV method. Figure 5 depicts representative CV curves of NiO nanopowders and NiO/NF hybrids measured at different scan rates of 5 mV/s, 10 mV/s, 20 mV/s and 50 mV/s in a potential range of −0.2 V–0.5 V (vs. Hg/HgO) in 6.0 M KOH electrolyte solution. It can be seen that the CV curves of NiO nanopowders don't present a regular rectangle, but present distortion of different degrees, confirming the Faradic nature of the NiO rather than EDLC, which is an ideal rectangular shape. The oxidation and reduction peaks of their respective anodic and cathodic scan are not symmetric, this is due to kinetic irreversibility of the redox process. The charge storage of NiO is expected to arise the following redox reaction:[39]

$$NiO + zOH^- \Leftrightarrow zNiOOH + (1\text{-}z)NiO + ze^- \quad (4)$$

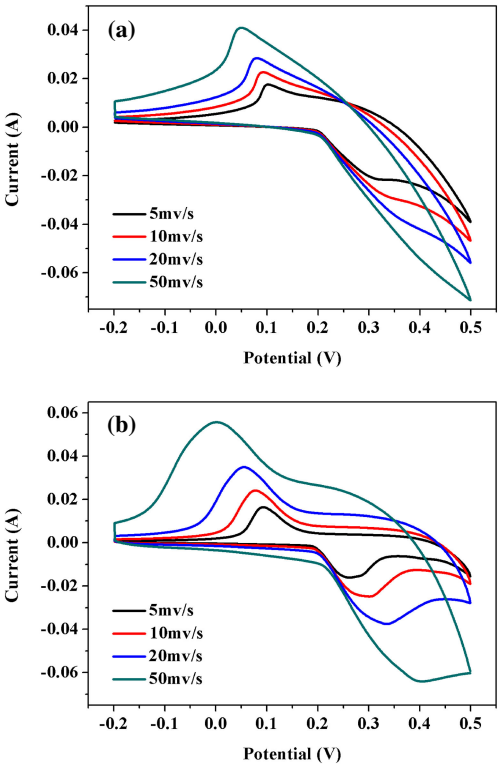

Figure 5. (Color online) CV curves of NiO nanopowders (a) and NiO/nickel foam hybrids (b).

In the process of charging, a large number of electric charges are stored in the electrode from Ni^{2+} into Ni^{3+}; in the process of discharging, the charged ions stored in the electrode back to the electrolyte and release through the external circuit from Ni^{2+} into Ni^{3+}. However, the CV curves of NiO nanopowders show that redox peaks are not obvious, indicating that the conductivity of the supercapacitor electrode material is poor. The faster of the scan rate, the more obvious of the redox peak; the higher of the redox potential, the more significantly distortion of CV curves. This is mainly because the poor conductivity of NiO leads to a decline in large current charge and discharge capacity. While the CV curves of NiO/NF hybrids show obvious redox peaks. As the scan rate increases from 5 mV/s to 50 mV/s, CV curves change just a little, indicating good conductivity and electrochemical stability of NiO/NF hybrids. Based on CV curves, the specific capacitances of NiO nanopowders are 85.4, 54.5, 33.5 and 16.8 F/g at different scan rates of 5, 10, 20, and 50 mV/s, respectively. While, the specific capacitances of NiO/NF hybrids are 234.8, 163.9, 122.0, 90.1 F/g at the same scan rates (Fig. 6). In conclusion, NiO/NF hybrids have excellent rate performance than NiO nanopowders due to their binder-free electrode structure.[40,41]

Figure 7 shows the Nyquist profiles of NiO nanopowder and NiO/NF hybrid in the frequency range of 0.01–500 kHz at a bias potential of 0.4 V. The inset shows the enlarged view of high frequency region. The impedance spectra include a slope line in the low-frequency and one semicircle in the high frequency, but these are not obviously in NiO nanopowders. The values of solution resistance (R_s) intercepted at high frequency on the real axis of these two electrodes are 3.6 Ω and 1.9 Ω, respectively. R_s is the combination of (i) ionic and electronic resistances, (ii) intrinsic resistance of the electrode, and (iii) diffusive as well as contact resistance at the NiO/nickel foam interface.[42] In addition, the values of charge transfer resistance (R_{ct}) corresponded the semicircle at high frequency region of these are 0.3 Ω and 0.25 Ω, respectively. These results may benefit from the structure of the ultrathin porous NiO nanoflake arrays, which enhances the diffusivity of the

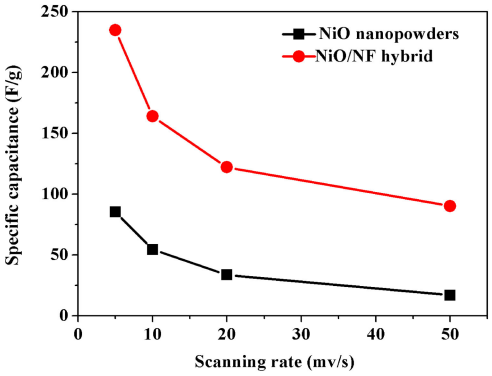

Figure 6. (Color online) the calculated specific capacitance of nanopowders (black) and NiO/nickel foam hybrids (red) as a function of scan rate.

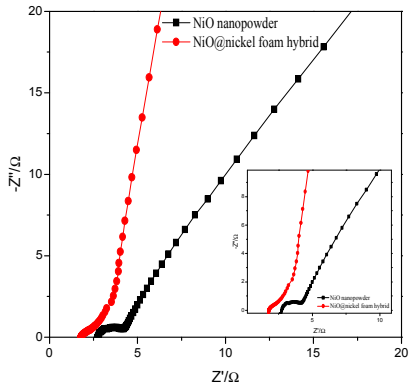

Figure 7. (Color online) EIS plots of the NiO nanopowder and NiO/nickel foam hybrid in 6.0 M KOH solution (Inset: the enlarged view of the high frequency region).

electrolyte, lowering the charge-transfer resistance value.[43] The smaller the charge transfer resistance, the faster the charge transfer result in good conductivity. In conclusion, the capacitance impedance characteristics of NiO/nickel foam hybrid are better than the NiO nanopowders and more suitable for electrode of high-performance supercapacitors.

4. Conclusions

In summary, NiO nanopowders were successfully synthesized and grown directly on nickel foam (NiO/nickel foam hybrid) by microwave hydrothermal method combined with the facile post heat treatment. NiO nanopowders have the morphology of microspheres with the diameter of about 3 μm, which are composed of porous nanoflakes. While NiO is grown directly on nickel foam, a porous nanoflakes array with the thickness of 10 nm is obtained. Benefiting from the rational structural features, NiO/NF hybrid as the binder-free electrode material for supercapacitors delivers the higher specific capacitance and exhibits more excellent conductivity than NiO nanopowders. Electrochemical studies indicate that the maximum specific capacitance of NiO nanopowders is about 85.4 F/g at scan rate of 5 mV/s, while this value is up to 234.8 F/g for NiO/nickel foam hybrid. The R_s and R_{ct} values of NiO array-based electrode are 1.9 Ω and 0.25 Ω, which are smaller than that of the sample for NiO nanopowder-based electrodes (3.6 Ω and 0.3 Ω). In conclusion, the ultrathin porous NiO nanoflake arrays on nickel foam with better electrochemical performance and excellent conductivity appear to be an up-and-coming electrode material for supercapacitors.

Acknowledgments

This work was supported by the National Natural Science Foundation from Shandong Province of China (ZR2012EMM005) and the Australian Research Council through a Discovery Project (project ID: DP0879070).

References

1. C. H. Wu and S. X. Deng, *J. Appl. Mater. Interfaces*, **6**, 1106 (2014).
2. A. Yoshida, S. Nonaka, I. Aoki, and A. Nishino, *J. Power Sources*, **60**, 213 (1996).
3. L. Q. Chen, *Batteries*, **30**, 98 (2000).
4. R. Wang and X. L. Miao, *Battery Industry*, **13**, 191 (2008).
5. G. H. Yuan, *Electrochemical Capacitors*, **2**, 23 (2006).
6. H. He, H. Liu, F. Liu, and K. C. Zhou, *Surf. Coat. Tech.*, **201**, 958 (2006).
7. H. Y. Wu and H. W. Wang, *Acta Phys. Chim. Sin.*, **29**, 1501 (2013).
8. X. Q. Tian, C. M. Cheng, L. Qian, B. Z. Zheng, H. Y. Yuan, S. P. Xie, D. Xiao, and M. M. Choi, *J. Mater. Chem.*, **22**, 8029 (2012).
9. G. Zhang, L. Yu, H. E. Hoster, and X. W. D. Lou, *Nanoscale*, **5**, 877 (2013).
10. X. H. Xia, J. P. Tu, Y. Q. Zhang, Y. J. Mai, X. L. Wang, C. D. Gu, and X. B. Zhao, *RSC Adv.*, **2**, 1835 (2012).
11. X. Liu, Q. Long, C. Jiang, B. Zhan, C. Li, S. Liu, Q. Zhao, W. Huang, and X. Dong, *Nanoscale*, **5**, 6525 (2013).
12. L. Mao, K. Zhang, H. S. O. Chan, and J. Wu, *J. Mater. Chem.*, **22**, 1845 (2012).
13. J. Zhu and J. He, *ACS Appl. Mater. Interfaces*, **4**, 1770 (2012).
14. C. Yuan, X. Zhang, L. Su, and B. Gao, *J. Mater. Chem.*, **19**, 5772 (2009).
15. D. L. Chen and L. Gao, *Chem. Phys. Lett.*, **405**, 159 (2005).
16. Z. X. Ding, W. M. Wu, S. J. Liang, H. R. Zheng, and L. Wu, *Mater. Lett.*, **65**, 1598 (2011).
17. L. X. Yang, Y. J. Zhu, H. Tong, Z. H. Liang, and W. W. Wang, *Cryst. Growth Des.*, **7**, 2716 (2007).
18. C. Z. Yang, X. G. Zhang, L. H. Shu, B. Gao, and L. F. Shen, *J. Mater. Chem.*, **19**, 5772 (2009).
19. Z. F. Zhu, N. Wei, H. Liu, and Z. L. He, *Adv. Powder Technol.*, **22**, 422 (2011).
20. Y. Wang, Q. S. Zhu, and H. G. Zhang, *Chem. Commun.*, **41**, 5231 (2005).
21. G. Duan, W. Cai, Y. Lou, and F. Sun, *Adv. Funct. Mater.*, **17**, 644 (2007).
22. Y. M. Li, W. Y. Li, S. L. Chou, and J. Chen, *J. Alloys Compd.*, **456**, 339 (2008).
23. D. B. Wang, C. X. Song, Z. S. Hu, and X. Fu, *Phys. Chem. B*, **1009**, 112 (2005).
24. M. S. Wu and M. J. Wang, *Chem. Commun.*, **46**, 6968 (2010).
25. X. M. Liu, X. G. Zhang, and S. Y. Fu, *Mater. Res. Bull.*, **41**, 620 (2006).
26. S. Vijayakumar, S. Nagamuthu, and G. Muralidharan, *ACS Appl. Mater. Interfaces*, **5**, 2188 (2013).
27. S. K. Meher, P. Justin, and R. G. Ranga, *Electrochim. Acta*, **55**, 8388 (2010).
28. J. Jiang, Y. Li, J. Liu, X. Huang, C. Yuan, and X. W. Lou, *Adv. Mater.*, **24**, 5166 (2012).
29. Y. Z. Zheng, H. Y. Ding, and M. L. Zhang, *Mater. Res. Bull.*, **44**, 403 (2009).
30. Y. L. Yuan, Z. W. Wang, J. S. Yu, and X. H. Guan, *J. Northeast Electric Power Univ.*, **29**, 29 (2009).
31. X. M. Liu, X. G. Zhang, and S. Y. Fu, *Mater. Res. Bull.*, **41**, 620 (2006).
32. M. A. Gondal, M. N. Sayeed, and Z. Seddigi, *J. Hazard. Mater.*, **155**, 83 (2008).
33. S. Faraji and F. N. Ani, *J. Power Sources*, **263**, 338 (2014).
34. D. D. Han, X. Y. Jing, J. Wang, P. C. Xu, L. Li, and J. X. Gong, *Inorg. Salt Industry*, **44**, 23 (2012).
35. J. Du, G. Zhou, H. M. Zhang, C. Cheng, J. M. Ma, W. F. Wei, L. B. Chen, and T. H. Wang, *ACS Appl. Mater. Interfaces*, **5**, 7405 (2013).
36. L. Qian, L. Gu, L. Yang, H. Y. Yuan, and D. Xiao, *Nanoscale*, **5**, 7388 (2013).
37. S. K. Meher and G. R. Rao, *ACS Appl. Mater. Interfaces*, **3**, 2063 (2011).
38. G. Q. Zhang and X. W. D. Lou, *Adv. Mater.*, **25**, 976 (2013).
39. S. Vijayakumar, S. Nagamuthu, and G. Muralidharan, *ACS Appl. Mater. Interfaces*, **5**, 2188 (2013).
40. X. Zhang, W. Shi, J. Zhu, W. Zhao, J. Ma, S. Mhaisalkar, T. L. Maria, Y. Yang, H. Zhang, H. H. Hng, and Q. Yan, *Nano Res.*, **3**, 643 (2010).
41. X. Sun, G. Wang, J. Y. Hwang, and J. Lian, *J. Mater. Chem.*, **21**, 16581 (2011).
42. T. Choudhury, S. O. Saied, J. L. Sullivan, and A. M. Abbot, *J. Phys. D: Appl. Phys.*, **22**, 1185 (1989).
43. J. H. Zhong, A. L. Wang, G. R. Li, J. W. Wang, Y. N. Ou, and Y. X. Tong, *J. Mater. Chem.*, **22**, 5656 (2012).